

Long-period body wave traveltimes through the crust: implication for crustal corrections and seismic tomography

J. Ritsema,¹ H. J. van Heijst,² J. H. Woodhouse² and A. Deuss³

¹Department of Geological Sciences, University of Michigan, Ann Arbor, MI 48109, USA. E-mail: jritsema@umich.edu

²Department of Earth Sciences, University of Oxford, Oxford OX1 3PR, UK

³Department of Earth Sciences, University of Cambridge, Cambridge CB3 0EZ, UK

Accepted 2009 August 13. Received 2009 August 12; in original form 2009 June 26

SUMMARY

The traveltimes of P and SH waves through the crust depend strongly on wave period. At periods longer than 10–15 s, where traveltimes measurements for indirect (e.g. surface reflected and core reflected) waves are typically made, the traveltimes are shorter than predicted by ray theory. Crustal corrections, often used in global mantle tomography to isolate the effects of the crust on teleseismic traveltimes, may have a complex frequency dependence and influence finite-frequency inversions.

Crustal corrections for profiles of CRUST2.0 and the PREM reference model for the mantle may be several seconds larger or smaller than ray-theoretical values, depending on crustal thickness, crustal velocities and wave period. This variability is observed in the difference times between the seismic phases SS and S and between PP and P . It is therefore important to incorporate the effects of the crust on traveltimes in finite-frequency tomography, in order to take full advantage of the variable mantle sensitivity of body waves at different periods.

Key words: Body waves; Seismic tomography; Wave propagation; Crustal structure.

1 INTRODUCTION

Body wave traveltimes are key data for tomographic imaging of small-scale seismic velocity variations in the deep Earth. To maximize body wave sampling of the mantle, it is necessary to include traveltimes for (multiple) surface reflections and core reflections in addition to direct P and S waves. These indirect body waves arrive within the coda of other phases. Moreover, their waveforms often lack clear onsets and may be distorted due to the effects of reflection, diffraction, and wave attenuation. Therefore, it is most practical to measure body wave traveltimes by waveform fitting (e.g. Vandecar & Crosson 1990; Grand 1994; Liu & Dziewonski 1996; Ritsema & van Heijst 2002; Sigloch & Nolet 2006; Houser *et al.* 2008) and preferably at frequencies lower than 0.1 Hz.

The crust has a profound influence on traveltimes. In global velocity models such as PREM (Dziewonski & Anderson 1981) and ak135 (Kennett *et al.* 1995), the shear velocity in the upper crust is 30 per cent lower than the uppermost mantle velocity. The variation in crustal thickness alone is responsible for several seconds of global one-way shear wave traveltime variation. Compared to direct S , the surface reflections SS and SSS propagate, respectively, two and four additional segments through the crust. For oceanic paths, SS and SSS propagate up to 5 s faster than predicted for the PREM because the oceanic crust is much thinner than modelled in PREM. Such anomalies are significant fractions of total teleseismic traveltime delays. It is thus important to account for the effects of the crust carefully when traveltimes are inverted for mantle structure.

Ideally, the (non-linear) effects of the crust are dealt with directly in the inversion. However, to simplify the inversion procedure, *a priori* corrections to the traveltimes are applied either by subtracting the expected crustal contributions from the traveltimes measurements or by absorbing the crustal traveltimes into ‘station terms’ (Cleary & Hales 1966; Dziewonski & Anderson 1983; VanDecar *et al.* 1995).

At relatively low frequencies, when the wavelengths of body waves are similar to the thicknesses of the crust, crustal traveltimes are frequency dependent. Yang & Shen (2006) discussed how the continental crust affects teleseismic P traveltimes. Here, we analyse transverse component S waves in addition to P and consider crustal structures for both oceans and continents. We analyse the effects in 1-D by modelling the crust as a layered structure and consider only teleseismic body waves.

In Section 2, we provide a theoretical basis for the finite frequency effects of crustal traveltimes at a single frequency. Although single-frequency and narrow-band measurements are improbable, the main characteristics of finite-frequency crustal traveltime variations that are discussed in Section 2 apply to wide-band ($f = 0.1$ – 0.02 Hz) measurements. This is demonstrated in Section 3 for the crustal structures from model CRUST2.0 (Bassin *et al.* 2000), which is often invoked as a model for the crust in global mantle tomography.

2 TRAVELTIMES IN LAYERED MEDIA

Wave propagation through layered media is a classic problem that can be conveniently cast using matrix algebra (Haskell 1953). We

will assume that teleseismic body-wave wave fronts are planes and follow the notation of Woodhouse (1981) who writes the relationship between the displacement–stress vector \mathbf{y} and its derivative with respect to depth z in a transversely isotropic material in the form

$$\frac{d\mathbf{y}}{dz} = \omega \mathbf{A}(p, z) \mathbf{y}, \quad (1)$$

where ω is the angular frequency, p is slowness. We derive in some detail expressions for *SH* waves for which the algebra is simpler. However, expressions for *P* traveltimes have in essence the same form.

2.1 *SH* waves

For *SH* waves \mathbf{y} has elements y_1 and y_2 representing transverse component displacement and shear stress, respectively. The matrix \mathbf{A} is a 2×2 matrix

$$\mathbf{A}(p, z) = \begin{pmatrix} 0 & L^{-1} \\ p^2 N - \rho & 0 \end{pmatrix}. \quad (2)$$

Here, ρ is density and $L = \rho V_{SV}^2$, $N = \rho V_{SH}^2$ are the elastic parameters of transversely isotropic material. \mathbf{A} is diagonalized by the matrix \mathbf{U} which has the eigenvectors of \mathbf{A} as columns

$$\mathbf{A} = \mathbf{U} \mathbf{\Lambda} \mathbf{U}^{-1}, \quad (3)$$

$$\mathbf{U} = \begin{pmatrix} 1 & 1 \\ i\eta L & -i\eta L \end{pmatrix}, \quad (4)$$

and

$$\mathbf{\Lambda} = \begin{pmatrix} i\eta & 0 \\ 0 & -i\eta \end{pmatrix}. \quad (5)$$

\mathbf{U} can be written as

$$\mathbf{U} = (\mathbf{u}^D \quad \mathbf{u}^U), \quad (6)$$

where \mathbf{u}^D and \mathbf{u}^U correspond to downward-propagating and upward-propagating *SH* waves, respectively. The vertical wavenumber is given by

$$\begin{aligned} \eta &= \sqrt{\frac{\rho}{L} - p^2 \frac{N}{L}} \\ &= \frac{V_{SH}}{V_{SV}} \sqrt{\frac{1}{V_{SH}^2} - p^2}. \end{aligned} \quad (7)$$

Consider the seismic structure of Fig. 1, where a layered zone with thickness H is overlying a homogeneous half-space with density ρ_2 and elastic parameters L_2 and N_2 , and an upward travelling wave and the reflected wave in the half-space, normalized to have unit amplitude and zero phase at a reference depth $z = s$. Thus,

$$\mathbf{y}(s) = \mathbf{u}^U e^{-i\omega\eta_2(z-s)} + r \mathbf{u}^D e^{i\omega\eta_2(z-s)}. \quad (8)$$

The displacement–stress vector \mathbf{y} at the surface can be written as

$$\mathbf{y}(0) = \mathbf{P}(0, H) \mathbf{y}(H) = \begin{pmatrix} P_{11} & P_{12} \\ P_{21} & P_{22} \end{pmatrix} \mathbf{y}(H), \quad (9)$$

where $\mathbf{P}(0, H)$ is the propagator matrix across the layered zone with elements P_{11} , P_{12} , P_{21} and P_{22} .

The reflection coefficient r is determined by the requirement that the stress component, $y_2(0)$, vanishes at the surface. We find that

$$r = \frac{P_{22} - P_{21}/i\eta_2 L_2}{P_{22} + P_{21}/i\eta_2 L_2} e^{-2i\omega\eta_2(H-s)} \quad (10)$$

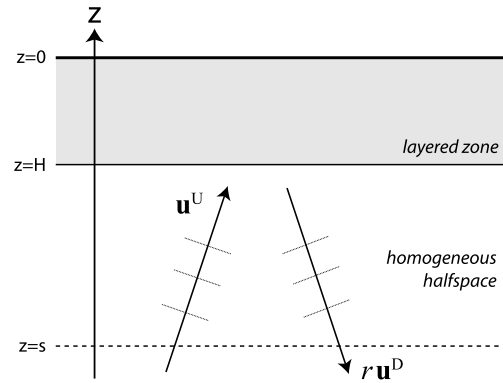


Figure 1. Sketch of wave propagation in a seismic model that includes a ‘layered zone’ with thickness H above a homogeneous half-space. The upward propagating plane *SH* wave, \mathbf{u}^U , has an amplitude of 1. The wave that has reflected off the layered zone, $r \mathbf{u}^D$, has an amplitude equal to r .

and the displacement at the surface

$$y_1(0) = \frac{2}{P_{22} + P_{21}/i\eta_2 L_2} e^{-i\omega\eta_2(H-s)}, \quad (11)$$

using the fact that $\det \mathbf{P}(H, s) = 1$. Therefore,

$$\arg y_1(0) = -\omega\eta_2(H-s) + \arctan\left(\frac{P_{21}}{\eta_2 L_2 P_{22}}\right) \quad (12)$$

and, hence, the traveltime through the layered zone between $z = 0$ and H

$$\Delta t = \omega^{-1} \arctan\left(\frac{P_{21}}{\eta_2 L_2 P_{22}}\right). \quad (13)$$

If the layered zone consists of a stack of homogeneous layers, then

$$\mathbf{P}(0, H) = \prod_{k=1}^K \begin{pmatrix} P_{11}^{(k)} & P_{12}^{(k)} \\ P_{21}^{(k)} & P_{22}^{(k)} \end{pmatrix}, \quad (14)$$

which represent successive left-multiplications of the propagator matrices for each layer k .

For a single homogeneous layer, with density ρ_1 and elastic parameters L_1 and N_1

$$\mathbf{P}(0, H) = \begin{pmatrix} \cos \omega H \eta_1 & (L_1 \eta_1)^{-1} \sin \omega H \eta_1 \\ -L_1 \eta_1 \sin \omega H \eta_1 & \cos \omega H \eta_1 \end{pmatrix} \quad (15)$$

and the time delay

$$\Delta t = \omega^{-1} \arctan(\sigma \tan \omega H \eta_1). \quad (16)$$

Here,

$$\sigma = \frac{L_1 \eta_1}{L_2 \eta_2} \quad (17)$$

is the ratio of the impedance in the layer and in the half-space. We define the ray-theoretical, or infinite-frequency, traveltime through the layer as

$$\Delta t_{\text{ray}} = H \eta_1 \quad (18)$$

and the normalized traveltime Δt_N as

$$\Delta t_N = \frac{\Delta t}{\Delta t_{\text{ray}}}. \quad (19)$$

If the seismic structure of the layer and the half-space are the same, then $\sigma = 1$ and $\Delta t_N = 1$. At sufficiently low frequencies (when $\omega \ll H \eta_1$) $\Delta t_N = \sigma$.

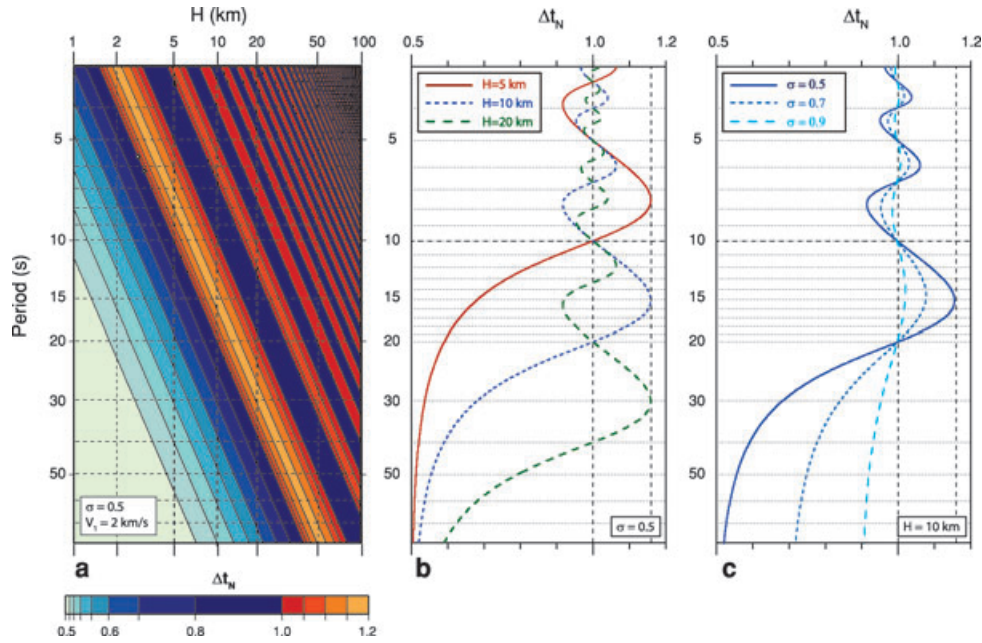


Figure 2. Δt_N for a structure comprised of homogeneous layer with a density $\rho_1 = 3.5 \text{ g cm}^{-3}$ and a shear velocity of $V_1 = 2.0 \text{ km s}^{-1}$ that is above a half-space with a density $\rho_2 = 3.5 \text{ g cm}^{-3}$. The shear velocity in the half-space $V_2 = 4.0 \text{ km s}^{-1}$, that is, $\sigma = 0.5$. Δt_N is plotted in (a) as a function of layer thickness H and wave period T and in (b) as a function of period for $H = 5, 10$ and 20 km . In (c), $H = 10 \text{ km}$ and Δt_N is plotted for $\sigma = 0.5, 0.7$ and 0.9 . We assume vertical wave propagation ($p = 0$).

2.2 Example

Let us consider a homogeneous layer with a density $\rho_1 = 3.5 \text{ g cm}^{-3}$ and a shear velocity of $V_1 = 2.0 \text{ km s}^{-1}$ that is above a half-space with a density $\rho_2 = 3.5 \text{ g cm}^{-3}$ and a shear velocity of $V_2 = 4.0 \text{ km s}^{-1}$. Let us further assume vertical wave incidence ($p = 0$) and isotropic shear velocities. Thus, $\eta_1 = 1/V_1$, $\eta_2 = 1/V_2$, $L_1 = N_1 = \rho_1 V_1^2$, $L_2 = N_2 = \rho_2 V_2^2$ and $\sigma = 0.5$.

Figs 2(a) and (b) illustrate the dependence of Δt_N on wave period T and layer thickness H . In Fig. 2(a), Δt_N is plotted as a function of layer thickness H and wave period T . Fig. 2(b) shows Δt_N as a function of period for values of H of 5, 10 and 20 km. These are the expected thicknesses for, for example, thick sedimentary basins, oceanic crust and thin continental crust.

At very short periods, when $T \ll \Delta t_{\text{ray}}$, $\Delta t_N = 1$, as expected for ray theory. Δt_N oscillates around 1 for periods T between Δt_{ray} and $4\Delta t_{\text{ray}}$ and has a maximum of 1.16 at period T of about $3\Delta t_{\text{ray}}$. Δt_N is lower than 1 at periods larger than $4\Delta t_{\text{ray}}$, and it approaches asymptotically a value equal to $\sigma = 0.5$ for $T \gg \Delta t_{\text{ray}}$.

Fig. 2(c) shows Δt_N for a 10-km-thick layer for three different values of σ . As expected, $\Delta t_N = 1$ for the ray-theoretical (i.e. infinite-frequency) limit for any value for σ and Δt_N approaches a value equal to σ for periods much larger than Δt_{ray} . The oscillations in Δt_N are strongest for the smallest values of σ , when the impedance contrasts between the layer and the half-space are strongest.

For realistic crustal structures, Δt_N may be significantly different from 1 when traveltimes are measured at periods comparable or larger than the ray-theoretical traveltime through the crust. Traveltimes through thin ($H < 5 \text{ km}$) sedimentary basins or ice sheets with low densities and low velocities are shorter than predicted by ray theory. Traveltimes through the oceanic crust can be determined accurately only using ray theory for periods less than 10 s. In addition, Δt_N varies with frequency within the 0.2–0.03 Hz band where body wave traveltimes are typically measured.

3 CRUST2.0 TRAVELTIMES

While Section 2 provides the theoretical basis for the frequency dependence of traveltimes through the (relatively thin) crust, we estimate the effects for a layered crust using synthetic waveforms calculated by normal-mode summation (Woodhouse 1988). This approach mimics the approach commonly used in global tomography in which traveltime anomalies are measured by comparing the waveforms of filtered body waves (or surface waves) to waveforms computed for a reference model (e.g. Grand 1994; Trampert & Woodhouse 1996; Ritsema & van Heijst 2002; Maggi *et al.* 2009).

We use PREM as the reference mantle model and CRUST2.0 (Bassin *et al.* 2000) as a model for the crust. CRUST2.0 represents the global crustal structure by 360 profiles at a $2^\circ \times 2^\circ$ scale. These 1-D profiles include layers of water, ice, sediments, and upper and lower crust. They are constrained by seismic experiments, published maps of sediments, and bathymetry and topography from ETOPO5 and averaged globally for similar geological and tectonic settings. We replace the (half-space) structure below the Moho by PREM's velocity structure.

Fig. 3 compares the density and shear velocity structure of PREM with profiles A0 and PE from CRUST2. Profile A0 has a 6.57-km-thick crust. It represents the crust beneath the oceans except in the vicinity of continental shelves and ocean islands. The crust in PE is 50 km thick and applies to orogenic regions, including northern Tibet.

3.1 Crustal corrections

We calculate synthetics for PREM and each of the CRUST2.0 profiles using normal-mode theory. A traveltime delay for a distinct body wave phase

$$\Delta t_C = T_{\text{CRUST2.0}} - T_{\text{PREM}} \Big|_{\text{one-way}} \quad (20)$$

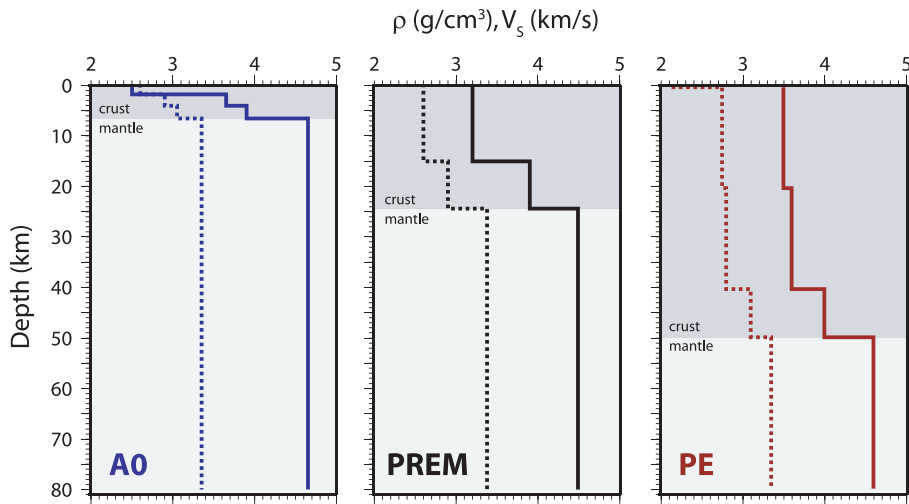


Figure 3. Shear velocity (solid line) and density (dashed line) profiles for PREM (black), and the profiles A0 ('normal oceanic') (blue) and PE ('orogen/50 km') (red) from model CRUST2.0.

is defined as the difference in traveltime for a single propagation segment through the crust for a CRUST2.0 profile and for PREM. Δt_C is entirely due to the difference in the crustal structure of CRUST2.0 and PREM. It is equivalent to a 'crustal correction' which, in tomography, is assumed to be the portion of the observed traveltime delay caused by the heterogeneous crust.

We measure Δt_C by cross-correlating the body-wave signals in the CRUST2.0 and the PREM synthetics using the procedures of Ritsema & van Heijst (2002). Synthetic seismograms for PE and A0 are compared to PREM seismograms in Fig. 4. The synthetics are lowpass filtered using corner frequencies ranging from 28 and 90 mHz. We adopt the source parameters for event 1996

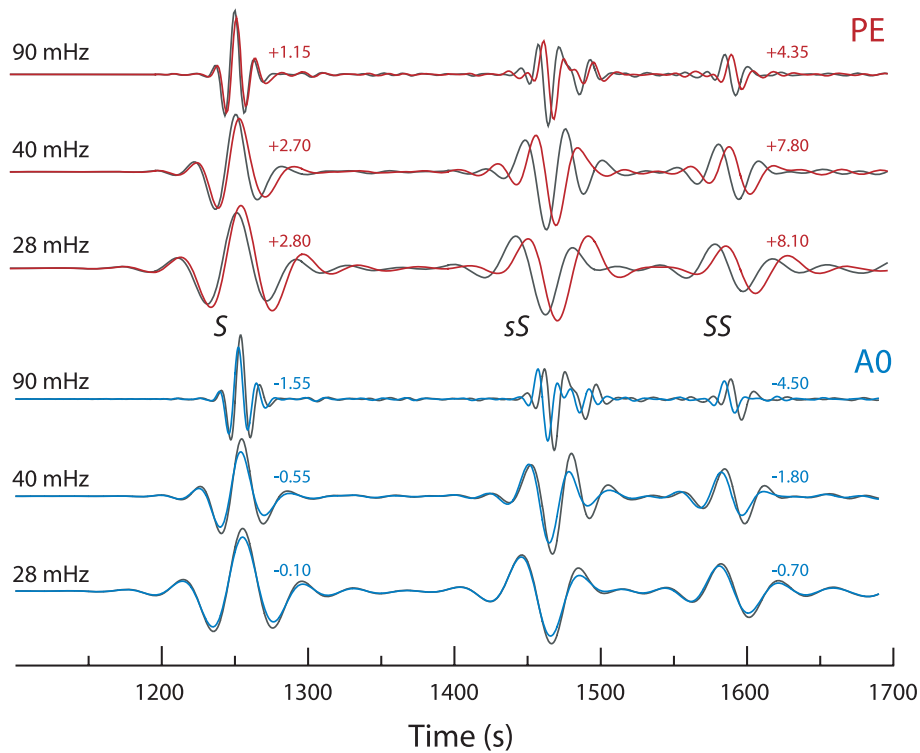


Figure 4. Synthetic seismograms for (black lines) PREM, and profiles (blue lines) A0 and (red lines) PE from CRUST2.0. The source parameters correspond to event 080596G from the CMT catalogue (1996 August 5; Tonga-Fiji region; $M_w = 7.4$; depth = 555 km). The transverse component seismograms are calculated for station COR (Corvallis, OR) at an epicentral distance of 82° and a source azimuth of 36° . The phases *S*, *sS* and *SS* are the largest amplitude signals between 1100 and 1700 s after the earthquake origin time. The seismograms are lowpass filtered using corner frequencies of (from top to bottom) 90 mHz ($T = 11$ s), 40 mHz ($T = 25$ s) and 28 mHz ($T = 36$ s). The delay (in seconds) of *S* and *SS* (with respect to PREM) is indicated above each trace.

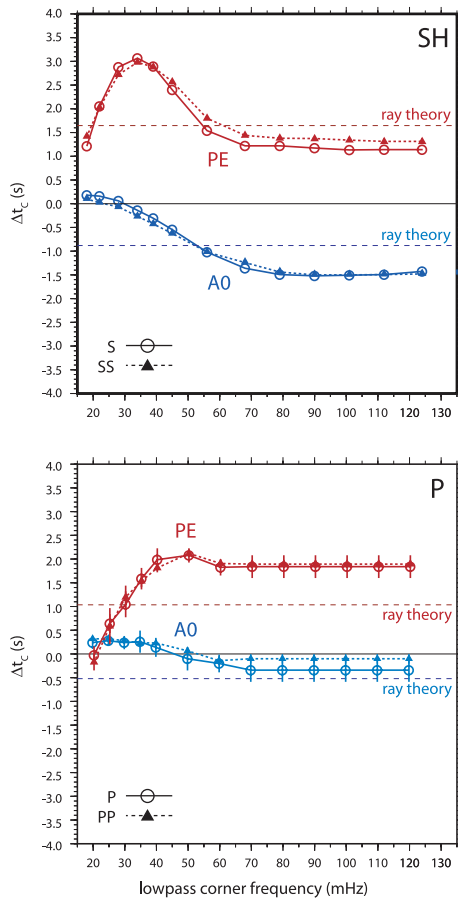


Figure 5. Δt_C for profiles (blue) A0 and (red) PE, for (top) S waves and (bottom) P waves. Δt_C is determined for direct waves (S and P) (solid lines and circles) and surface reflected waves (SS and PP) waves (dashed lines and triangles). Note that we define Δt_C as a one-way traveltimes through the crust. Actual delays of SS and PP are three times larger than S and P delays, respectively.

August 5 ($M_w = 7.4$, source depth = 555 km) from the Global CMT catalogue and compute waveforms for station COR (Corvalis, Oregon) at an epicentral distance of $\Delta = 82^\circ$ and a source azimuth of $\phi = 36^\circ$.

The seismograms show the expected delays in S, sS and SS. These shear waves propagate slower through profile PE, which has a thicker crust than PREM, than through PREM. For profile A0, which has a thinner crust than PREM, S, sS and SS arrive relatively early. Since SS and sS have two additional propagation segments through the crust, their traveltimes are approximately three times larger than the S delay.

Fig. 5 shows Δt_C as a function of lowpass corner frequency. Many of the trends in Δt_C are akin to the arctan functional shape as discussed in Section 2.2 although a direct comparison between Figs 2 and 5 is not straightforward since profiles PE and A0 are not homogeneous and Δt_C is not a single-frequency measurement.

For both P and SH and for both A0 and PE (and other profiles) the crustal correction Δt_C approaches zero for very low frequencies, indicating that the influence of the crust diminishes at the longest wavelengths. However, across the entire frequency band examined, Δt_C is different from ray-theoretical values, due to the dominating presence of relatively low-frequency signals in the passband.

SH traveltimes through the relatively thin crust of A0 are short compared to the ray-theoretical traveltimes. Hence, Δt_C is more

negative than expected according to ray theory. The trend of Δt_C is similar to shape of Δt_N in Fig. 2(b) for the ‘ $H = 5$ km’ profile, for periods T that are at least four times larger than the ray-theoretical one-way traveltimes (Δt_{ray}) through the crust.

In contrast, Δt_C is, in absolute sense, smaller than expected for ray theory for profile PE. In this case, the measured traveltimes through PREM (which has a thinner crust than PE) is smaller than expected for ray theory. Note also that Δt_C for SH traveltimes through PE has a maximum near 35 mHz, or a period of 30 s. This period is approximately $2.2 \times$ the ray-theoretical traveltimes Δt_{ray} through the PE crust. The maximum is observed at a lower period than the expected $3 \times \Delta t_{\text{ray}}$ (see Fig. 2) because the crust of PE is layered and because Δt_C for PE is determined using synthetics over a broad range of frequencies.

Fig. 5 also demonstrates that Δt_C depends little on ray parameter for teleseismic distances. Differences between one-way traveltimes delays determined for S and SS are largest when the crust is thick and when waveforms are analysed at the highest frequencies. For PE, Δt_C determined from SS and S differs by 0.23 s. At an epicentral distance of 82° , SS and S have incidence angles at the base of the crust of about 27° and 41° , respectively.

3.2 Maps of SH and P traveltimes through CRUST2.0

Values for Δt_C for all profiles of CRUST2.0 are shown in map view in Fig. 6. The traveltimes are measured for three low-pass corner frequencies: 28, 40, 90 mHz and computed using ray-theory. Profile A0 applies to most of the oceanic regions, thus the trend in Δt_C in the oceans is identical to the A0 profile shown in Fig. 5. For SH, Δt_C is negative because oceanic crust is thinner than the crust in PREM. In absolute value, Δt_C for the oceans decreases with decreasing frequency as the influence of the relatively thin oceanic crust on the SH traveltimes delay diminishes. For P waves, Δt_C in the ocean changes sign. It is -0.34 s for a low pass frequency of 90 mHz, $+0.15$ s and $+0.22$ s for low pass frequencies of, respectively, 40 and 28 mHz. This behaviour for P waves is due to the fact that P velocities are higher than SH velocities and due to the interaction of P waves with the ocean.

The crustal correction for continents is positive since continental crust is thicker than the crust in PREM. Contrary to the oceanic corrections, the magnitude of the correction increases with decreasing frequency because the influence of the continental crust on traveltimes is relatively high compared to the (now relatively thin) PREM crust. This is especially obvious for orogenic regions such as Tibet, where the crust is as thick as 70 km.

3.3 Observations of SS-S and PP-P

The frequency-dependent crustal corrections can be observed in recorded traveltimes differences of SS and S (SS-S) and PP and P (PP-P). SS-S and PP-P are not affected by earthquake mislocation and origin time errors nor by crust and upper mantle heterogeneity beneath the source and receiver where SS (PP) and S (P) have similar propagation paths. Since heterogeneity in the lower mantle is relatively weak, SS-S and PP-P are primarily affected by crust and uppermost mantle structure beneath the SS and PP surface reflection points (e.g. Woodward & Masters 1991).

Fig. 7 compares SS-S and PP-P measurements made by cross-correlating recordings and PREM synthetics that are lowpass filtered using corner frequencies of 28 mHz (x -axis) and 90 mHz (y -axis). SS-S and PP-P are separated into two groups: Figs 7(a) and (b) show measurements for which SS (and PP) have surface

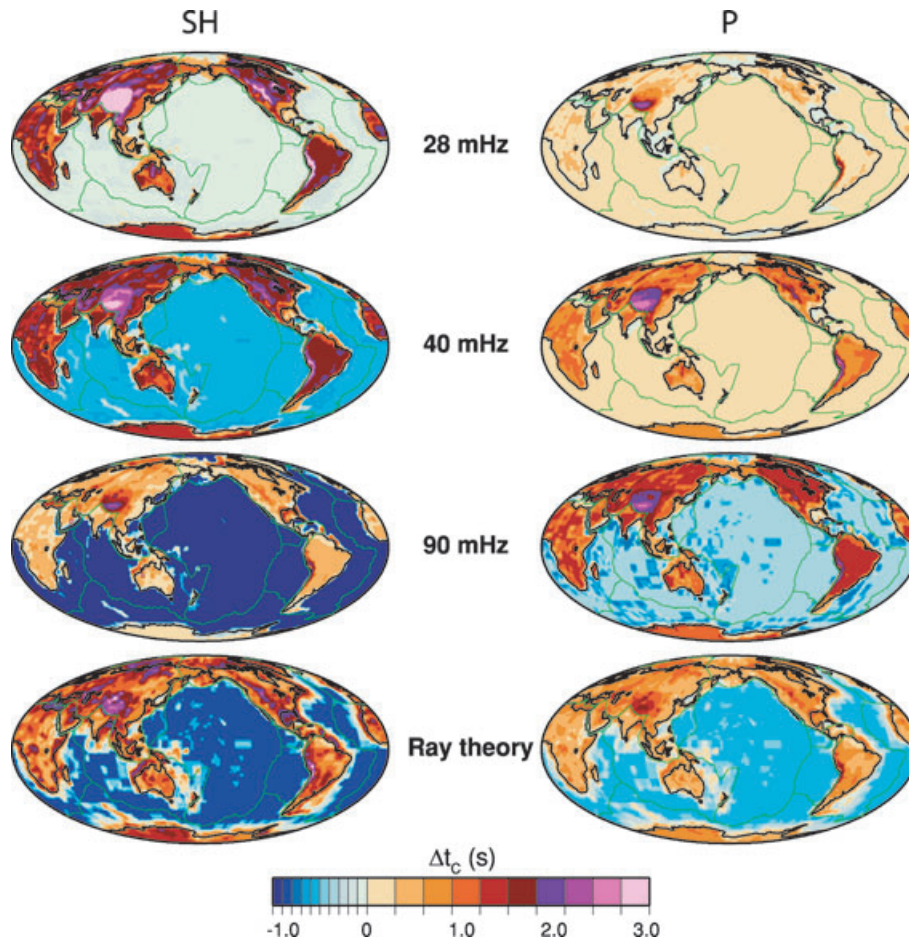


Figure 6. Δt_C for the 1-D profiles of CRUST2.0 for (left-hand side) *SH* waves and (right-hand side) *P* waves. The upper three panels are determined using waveform analysis of lowpass filtered synthetics for corner frequencies of 28, 40 and 90 mHz. The panel at the bottom is computed using ray theory.

reflection points beneath the oceans while Figs 7(c) and (d) show SS-S and PP-P for continental SS reflection points. These data exhibit a clear ocean/continent signal, indicating that SS-S and PP-P are signatures primarily of the velocity structure below the SS and PP surface reflection points. SS-S is predominantly negative (i.e. SS arrives earlier than expected for PREM) for oceanic SS reflection points and predominantly positive for continental SS reflection points. The same signal is observed for PP-P although PP-P is about two to three times smaller than SS-S.

While the continental SS-S measurements at 28 and 90 mHz scatter about the line $y = x$, the oceanic SS-S and PP-P are, on average, smaller by about 1 s at the lowest frequency. This offset in the data is due to the frequency dependence of the SS and PP traveltimes. At the lowest frequency, the traveltime delays of SS and PP through the thin oceanic crust are smaller than predicted by ray theory. On the other hand, the delay through the PREM crust is closer to the ray theoretical values. The frequency dependence of SS-S and PP-P is much smaller (and poorly recorded by our data) for continental SS and PP reflection points since the structure of the crust in PREM is more compatible with the continental crust.

4 DISCUSSION AND CONCLUSIONS

The maps of crustal corrections for CRUST2.0 in Fig. 6 depend on choices made in the measurement procedure (e.g. length and shape of body wave cross-correlation windows, or shape of low pass fil-

ters). Nevertheless, the frequency dependence of Δt_C is a robust attribute when body-wave traveltimes are measured at periods that are comparable or larger than the one-way traveltime through the crust, irrespective of the detailed traveltime measurement procedure. The frequency dependence is observable in high-quality measurements of traveltimes based on waveform fitting. Ray-theoretical values of crustal corrections may be larger or smaller than finite-frequency estimates, depending on crustal structure and the dominant wave period.

It is our experience that the resolution of long-wavelength (>2000–3000 km) structure changes little when finite-frequency crust corrections are used instead of ray-theoretical corrections. However, to achieve high-resolution of deep mantle heterogeneity it is important to carefully consider the effects of the crust when the fit to traveltimes delays by finite-frequency and ray-theoretical tomographic model are compared (e.g. Montelli *et al.* 2004) or when traveltime measurements in different frequency bands are inverted (Sigloch *et al.* 2008).

ACKNOWLEDGMENTS

This research has been funded by NSF grant EAR-0609763. We thank Gabi Laske for providing us model CRUST2.0 via (<http://mahi.ucsd.edu/Gabi/crust2.html>). We thank Barbara Romanowicz and an anonymous reviewer for constructive comments that helped us improve the manuscript. Data have been provided by

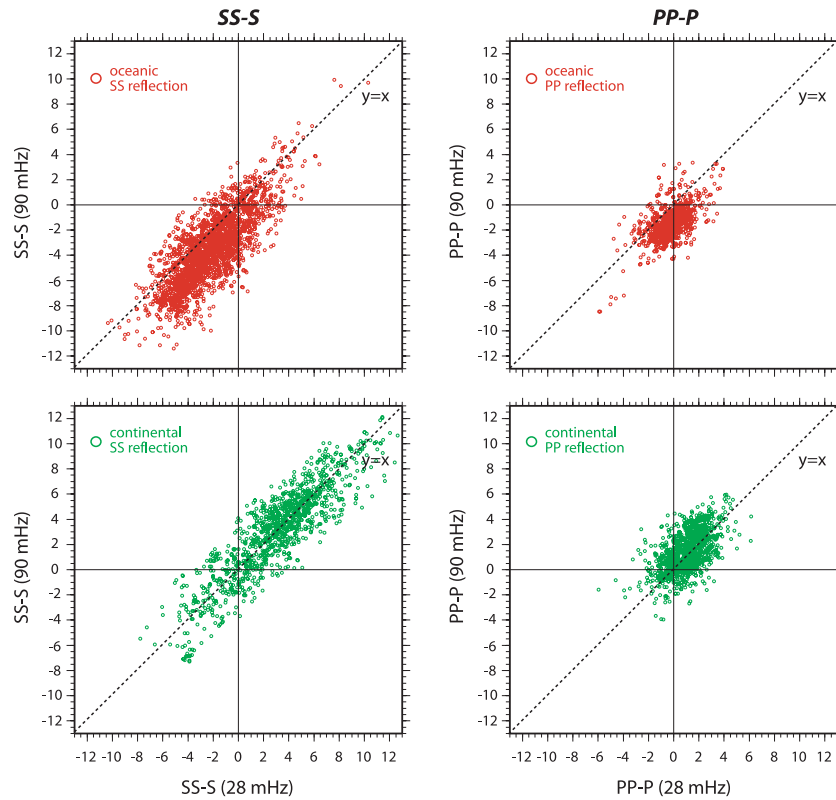


Figure 7. Measurements of (left-hand side) SS-S and (right-hand side) PP-P difference times with respect to PREM using lowpass filtered waveforms with corner frequencies of (x -axis) 28 mHz and (y -axis) 90 mHz. The red and green circles represent measurements for SS and PP surface reflection points beneath the oceans and continents, respectively. The dashed line is the function $y = x$.

the IRIS/DMC and the Geoscope Data Center. Figures have been produced using the GMT software of Wessel & Smith (1995).

REFERENCES

- Bassin, C., Laske, G. & Masters, G., 2000. The current limits of resolution for surface wave tomography in North America, *EOS, Trans. Am. geophys. Un.*, **81**, F897.
- Cleary, J. & Hales, A.L., 1966. An analysis of the travel times of P waves to North American stations, in the distance range 32° to 100° , *Bull. seism. Soc. Am.*, **56**, 467–489.
- Dziewonski, A.M. & Anderson, D.L., 1981. Preliminary Reference Earth Model, *Phys. Earth planet. Int.*, **25**, 297–356.
- Dziewonski, A.M. & Anderson, D.L., 1983. Travel-times and station corrections for P-waves at teleseismic distances, *J. geophys. Res.*, **88**, 3295–3314.
- Grand, S.P., 1994. Shear mantle structure beneath the Americas and the surrounding oceans, *J. geophys. Res.*, **99**, 11 591–11 621.
- Haskell, N.A., 1953. The dispersion of surface waves in multilayered media, *Bull. seism. Soc. Am.*, **43**, 17–34.
- Houser, C., Masters, G., Shearer, P. & Laske, G., 2008. Shear and compressional velocity models of the mantle from cluster analysis of long-period waveforms, *Geophys. J. Int.*, **174**, 195–212.
- Kennett, B.L.N., Engdahl, E.R. & Buland, R., 1995. Constraints on seismic velocities in the Earth from traveltimes, *Geophys. J. Int.*, **122**, 108–124.
- Liu, X.F. & Dziewonski, A.M., 1996. Global analysis of shear wave velocity anomalies in the lowermost mantle, in *The Core-Mantle Boundary Region*, Vol. **28**, pp. 21–36, Geodynamics Series, American Geophysical Union.
- Maggi, A., Tape, C., Chen, M., Chao, D. & Tromp, J., 2009. An automated data-window selection algorithm for adjoint tomography, *Geophys. J. Int.*, **178**, 257–281.
- Montelli, R., Nolet, G., Masters, G., Dahlen, F.A. & Hung, S.-H., 2004. Global P and PP traveltimes tomography: rays versus waves, *Geophys. J. Int.*, **158**, 637–654.
- Ritsema, J. & van Heijst, H.J., 2002. Constraints on the correlation of P- and S-wave velocity heterogeneity in the mantle from P, PP, PPP, and PKPab traveltimes, *Geophys. J. Int.*, **149**, 482–489.
- Sigloch, K. & Nolet, G., 2006. Measuring finite-frequency body-wave amplitudes and traveltimes, *Geophys. J. Int.*, **167**, 271–287.
- Sigloch, K., McQuarrie, N. & Nolet, G., 2008. Two-stage subduction history under North America inferred from multiple-frequency tomography, *Nat. Geosci.*, **1**, 458–462.
- Trampert, J. & Woodhouse, J.H., 1996. High-resolution global phase-velocity distributions, *Geophys. Res. Lett.*, **23**, 21–24.
- Vandecar, J.C. & Crosson, R.S., 1990. Determination of teleseismic relative phase arrival times using multi-channel cross-correlation and least-squares, *Bull. seism. Soc. Am.*, **80**, 150–169.
- VanDecar, J.C., James, D.E. & Assumpcao, M., 1995. Seismic evidence for a fossil mantle plume beneath South America and implications for plate driving forces, *Nature*, **378**, 25–31.
- Wessel, P. & Smith, W.H.F., 1995. New version of the generic mapping tools released, *EOS, Trans. Am. geophys. Un.*, **76**, 329.
- Woodhouse, J.H., 1981. A note on the calculation of travel times in a transversely isotropic earth model, *Phys. Earth planet. Inter.*, **25**, 357–359.
- Woodhouse, J.H., 1988. The calculation of the eigenfrequencies and eigenfunctions of the free oscillations of the Earth and the Sun, in *Seismological Algorithms*, pp. 321–370, Academic Press, London.
- Woodward, R.L. & Masters, G., 1991. Global upper mantle structure from long-period differential travel-times, *J. geophys. Res.*, **96**(B4), 6351–6377.
- Yang, T. & Shen, Y., 2006. Frequency-dependent crustal correction for finite-frequency seismic tomography, *Bull. seism. Soc. Am.*, **96**, 2441–2448.